Inorganic Chemistry

Article

pubs.acs.org/IC

Influence of Selenocyanate Ligands on the Transition Temperature and Cooperativity of bapbpy-Based Fe(II) Spin-Crossover Compounds

Sipeng Zheng,[†] Maxime A. Siegler,[‡] Olivier Roubeau,[§] and Sylvestre Bonnet*[,†]

[†]Leiden Institute of Chemistry, Gorlaeus Laboratories, Leiden University, P.O. Box 9502, Leiden, 2300 RA, The Netherlands

[‡]Small Molecule X-ray Facility, Department of Chemistry, Johns Hopkins University, Baltimore, Maryland 21218, United States

[§]Instituto de Ciencia de Materiales de Aragón (ICMA), CSIC and Universidad de Zaragoza, Plaza San Francisco s/n, 50009 Zaragoza, Spain

Supporting Information

ABSTRACT: Coordination of the ligand bapbpy (**1**, bapbpy = *N*,*N*′-di(pyrid-2-yl)-2,2′-bipyridine-6,6′-diamine), of one of its four dimethyl-substituted analogues **2**–**5** (R_2bapbpy = *N*,*N*′-di(methylpyrid-2-yl)-2,2′-bipyridine-6,6′-diamine), or of one of its three bis(iso)quinoline analogues **6**–**8** (R_2bapbpy= *N*,*N*′-di(quinolyl)-2,2′-bipyridine-6,6′-diamine), to $Fe(NCSe)_2$, afforded eight new iron(II) compounds of the type $[Fe(R_2bapbpy)(NCSe)_2]$ (**9**–**16**). Three of these compounds (**11**, **13**, and **16**) were structurally characterized by single crystal X-ray diffraction, which showed similar molecular geometry and packing compared to their thiocyanate analogues. Magnetic susceptibility measurements were carried out for all iron compounds and revealed thermal spin-crossover (SCO) behavior for compounds **9**, **11**, **13**, **15**, and **16**. Compounds **11**, **13**, **15**, and **16** show an increased transition temperature compared to the thiocyanate analogues. $[Fe(bapbpy)(NCSe)_2]$ (**9**) shows a gradual, one-step SCO, whereas its thiocyanate analogue $[Fe(bapbpy)(NCS)_2]$ is known for its cooperative two-step SCO. To discuss the influence of S-to-Se substitution on the cooperativity of the SCO, heat capacity measurements were carried out for compounds **9**, **11**, **13**, **15**, and **16**, and fitted to the Sorai domain model. The number *n* of like-spin SCO centers per interacting domain, which is a quantitative measure of the cooperativity of the spin transition, was found to be high for compounds **11** and **15**, and low for compounds **9**, **11**, and **13**. Compound **15** is one of the few known SCO compounds that is more cooperative than its thiocyanate analogue. Altogether, X-ray diffraction, calorimetry, and magnetic data give a consistent structure–property relationship for this family of compounds: hydrogen-bonding networks made of intermolecular N–H···Se interactions are of paramount importance for the cooperativity of the SCO.

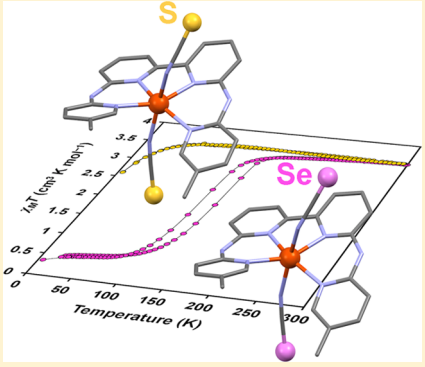

INTRODUCTION

There is a large scientific and technological interest in finding new molecular switches, as they could be used for nanosized gas sensors,[1,2] anion sensors,[3−5] temperature sensors,[6] actuators,[7] or data storage devices.[8−11] Spin-crossover (SCO) iron(II) complexes are typical prototypes of molecular switches,[12,13] as they reversibly transit between the low-spin (LS) and high-spin (HS) states upon temperature or pressure variations, upon light irradiation, or under the influence of strong magnetic or electric fields.[14−16] Besides the temperature at which the SCO occurs, the cooperativity of the transition is an important characteristic of SCO that results from the existence of short- and long-range intermolecular interactions in the crystal lattice. However, it still remains very challenging to design SCO materials featuring predefined properties, e.g., with cooperative SCO transitions occurring near or above room-temperature.

The thermal SCO phenomenon is usually rationalized within the frame of the ligand field theory.[17] In this model strongly coordinating ligands generate a higher ligand field splitting in the metal complex, as a result of which the low-spin (LS) state of the metal center is stabilized, and hence, the transition temperature $T_{1/2}$ of the SCO compound is increased. Within the widely used series of N-bound cyanate-derived ligands NCX^- (X = O, S, Se), the selenocyanate ligands are known to increase the ligand field splitting compared to thiocyanates as selenium is slightly less electronegative than sulfur (and thus electron withdrawal from the N atom is slightly lesser for Se). Consistently, from the first studies on the classical systems $[Fe(L)_2(NCX)_2]$ (where L = phen or 2,2′-bipy and X = S, Se),[18−20] to the more recent examples based on the 1,2,4-triazole ligand,[21,22] it has been shown that, with the increase of the ligand field splitting along the NCX^- (X = O, S, Se) spectrochemical series, the transition temperature $T_{1/2}$ indeed shifts toward higher temperatures. Quantitative data on the influence of sulfur-to-selenium replacement on the cooperativity of SCO are scarcer, either

Received: September 29, 2014
Published: November 20, 2014

because the single crystal structure of one of the analogues is missing, or because quantification of the cooperativity, for example through the simulation of calorimetry data, has not been systematically done.[23,24]

We recently reported the two-step mononuclear SCO compound $[Fe(bapbpy)(NCS)_2]$[25] (**1**, bapbpy = *N*,*N*′-di-(pyrid-2-yl)-2,2′-bipyridine-6,6′-diamine, see Scheme 1) and

Scheme 1. Structure of the Ligand bapbpy (1) and of Its Derivatives 2−8

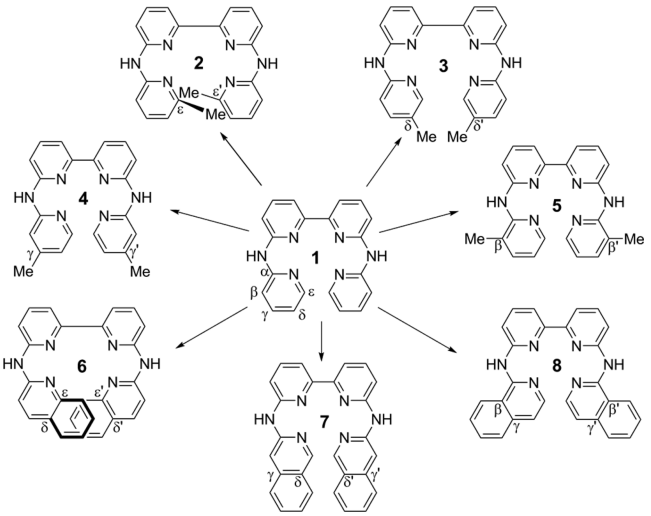

seven derivatives $[Fe(R_2bapbpy)(NCS)_2]$ with different substituents on the terminal pyridine rings of the bapbpy ligand (Scheme 1).[26] The crystal structures determined for this family of compounds showed that the thiocyanate sulfur atoms play a major role in the cooperativity of the SCO, as only strong intermolecular N−H···S hydrogen-bonding interactions lead to cooperative SCO. This important feature opened a unique opportunity to study the influence of exchanging S by Se on the cooperativity of the SCO. Designing SCO materials is indeed very difficult as minor chemical changes of the ligands often lead to significant changes in the SCO properties of the material. For example, modifying the chemical structure of the ligands R_2bapbpy in $[Fe(R_2bapbpy)(NCS)_2]$ allowed for increasing the transition temperature of the SCO near room-temperature, but at the cost of cooperativity.[26] The present study reports on the substitution of the axial NCS^- ligands in $[Fe(R_2bapbpy)(NCS)_2]$ complexes by $NCSe^-$, and on the effects of such replacement on the occurrence, transition temperature, and cooperativity of the SCO.

RESULTS

Synthesis of the Complexes. The ligand bapbpy (**1**) and seven derivatives **2**−**8** were synthesized according to the literature.[25,26] Coordination of these ligands to iron(II) bis(selenocyanate) was achieved using three different methods, hereafter called methods **a**−**c**. Method **a** has been previously described[25] and consists of impregnating a methanolic suspension of the ligand by a methanol solution of $Fe(NCSe)_2$. The advantage of this method is that the materials are obtained in high yields (>80%), but one drawback is that the materials may contain variable amounts of the free ligand, as exemplified by the inconsistency between the calculated and experimental values found by elemental analyses for compound **9a** and **11a** (no further elemental analyses were performed on other samples of type a). In method **b**, the ligand was first dissolved in DMF, before addition of 1.1 equiv of $Fe(NCSe)_2$ as a methanolic solution. Because the metal compounds are poorly soluble in pure methanol, their solubility is lowered as methanol slowly diffuses into the DMF solution, leading to precipitation of the complexes. This method usually results in a higher chemical purity compared to method **a**, unless the starting ligand is poorly soluble in DMF. Finally, method **c** is similar to method **b**, but methanol diffusion is slowed down to obtain single crystals of the iron compounds, whereas both methods **a** and **b** produce polycrystalline powders. In this work, compounds **9a**−**16a** were synthesized via method **a**, and only compounds **9b**, **11b**, **13b**, **15b** were synthesized by method **b**, due to the low solubility of the ligands **2**, **4**, **6**, and **8** in DMF (see Table 1 for formulation of all compounds). Finally, three ligands led to the formation of single crystals called **11c**, **13c**, and **16c** that were suitable for X-ray structure determination.

Table 1. Numbering, Formulae, Infrared Selenocyanate Stretching Vibrations, and HR-MS $[Fe(R_2bapbpy)(NCSe)]^+$ Monocationic Peak, for Compounds 9−16

compd/ method	formula	$NCSe^-$ vibrations (cm^{-1})	*m*/*z*
9a	*trans*-$[Fe(\mathbf{1})(NCSe)_2]$	2090, 2057	501.9978
9b	*trans*-$[Fe(\mathbf{1})(NCSe)_2]\cdot 2DMF$	2067	501.9973
10a	*trans*-$[Fe(\mathbf{2})(NCSe)_2]$	2057	530.0288
11a	*trans*-$[Fe(\mathbf{3})(NCSe)_2]$	2094, 2060	530.1[a]
11b	*trans*-$[Fe(\mathbf{3})(NCSe)_2]$	2093, 2052	530.0290
12a	*trans*-$[Fe(\mathbf{4})(NCSe)_2]$	2080	530.1[a]
13a	*trans*-$[Fe(\mathbf{5})(NCSe)_2]$	2100, 2070	530.0282
13b	*trans*-$[Fe(\mathbf{5})(NCSe)_2]$	2100, 2066	530.0294
14a	*trans*-$[Fe(\mathbf{6})(NCSe)_2]$	2078	602.1[a]
15a	*trans*-$[Fe(\mathbf{7})(NCSe)_2]$	2061	602.0287
15b	*trans*-$[Fe(\mathbf{7})(NCSe)_2]$	2060	602.0286
16a	*trans*-$[Fe(\mathbf{8})(NCSe)_2]$	2108, 2072	602.0290

[a]Measured by standard ESI-MS.

All new materials were analyzed with IR spectroscopy and mass spectrometry. The expected $[Fe(R_2bapbpy)(NCSe)]^+$ monocationic peak was found by electron-spray mass spectrometry (calculated at *m*/*z* 502 for **9**, 530 for **10**−**13**, and 602 for **14**−**16**; see Table 1), which confirmed coordination of the ligands to Fe(II). Consistently, the IR spectra of the 13 solids showed the characteristic stretching vibrations of the coordinated selenocyanate ligands in the range 2060−2100 cm^{-1} (Table 1). For compounds **9a**, **11a**, **11b**, **13a**, **13b**, **16a**, and **16c**, another $NCSe^-$ stretching vibration was observed in the range 2052−2074 cm^{-1}. It is worth noticing that **9b** shows an intense absorption band at 1661 cm^{-1}, which is not present in the infrared spectrum of **9a**. This absorption band is most likely due to the presence of DMF molecules in the crystal lattice of **9b**. Elemental analyses indeed account for two DMF molecules per iron complex in the crystal lattice of **9b**, whereas compounds **11b**, **13b**, and **15b** do not have any lattice solvent molecule.

Single Crystal and Powder X-ray Diffraction Studies. Single crystals of compounds **11**, **13**, and **16** suitable for X-ray structure determination were obtained via method **c**. A mixture of dark orange and dark red crystals was obtained for compound **11**. X-ray structure determination showed that the dark red crystals are solvent free (compound **11c**), whereas the dark orange crystals (compound **11c**′) contain one methanol molecule per iron complex. When crystals of **11c** were either

dx.doi.org/10.1021/ic502381m | Inorg. Chem. 2014, 53, 13162−13173

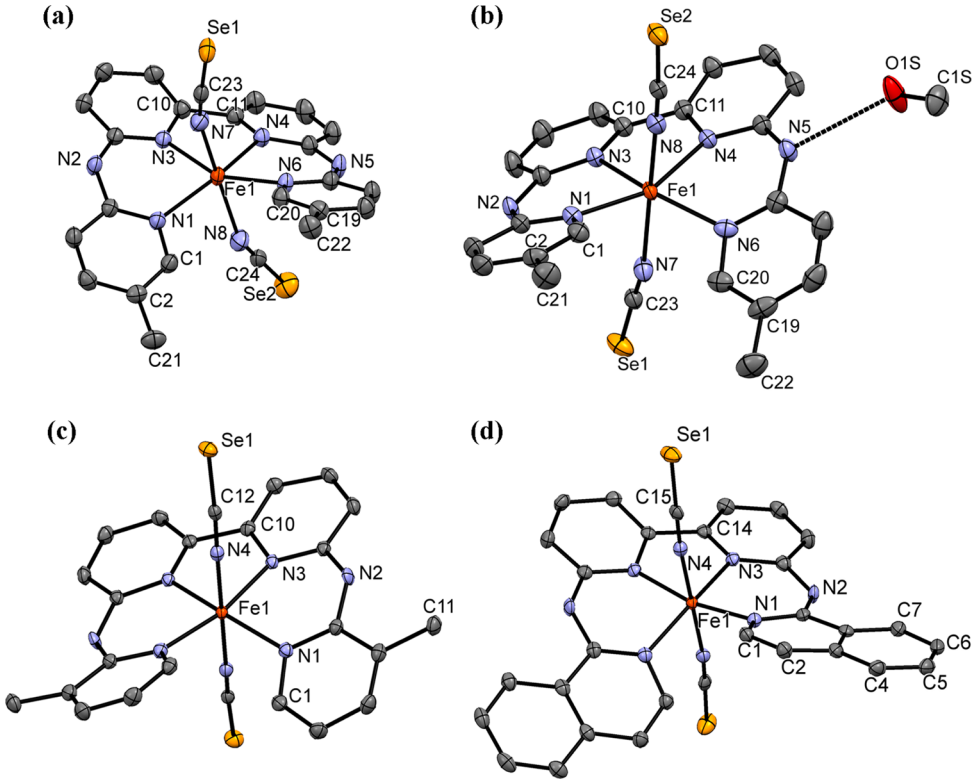

Figure 1. Displacement ellipsoid plots (50% probability level) (a) for compound **11c** at 200(2) K (HS phase), (b) for **11c′** at 110(2) K (HS phase), (c) for compound **13c** at 102(2) K (LS phase), (d) for compound **16c** at 110(2) K (LS phase). Hydrogen atoms were omitted for clarity. Selected atom labeling is only shown for crystallographically independent atoms.

Table 2. Selected Bond Lengths (Å) and Angles (deg) for the Crystal Structures of 11c, 11c′, 13c (HS and LS Phases), and 16c

	11c	**11c′**		**13c**		**16c**
T (K)	200(2)	110(2)		300(2)	102(2)	110(2)
phase	HS	HS		HS	LS	LS
Fe1−N1	2.1518(17)	2.1340(19)	Fe1−N1	2.126(3)	2.0221(18)	2.002(2)
Fe1−N3	2.1567(16)	2.1300(18)	Fe1−N3	2.108(2)	1.9500(18)	1.947(2)
Fe1−N4	2.1547(17)	2.1219(18)	Fe1−N4	2.144(3)	1.9470(19)	1.951(2)
Fe1−N6	2.1630(17)	2.130(2)	N1−Fe1−N1	110.13(15)	97.49(11)	96.50(13)
Fe1−N7	2.1831(19)	2.153(2)	N1−Fe1−N4	86.92(11)	87.35(7)	85.00(9)
				93.34(11)	94.09(8)	96.03(9)
Fe1−N8	2.1518(19)	2.132(2)	N3−Fe1−N1	86.56(10)	90.65(7)	91.30(9)
N1−Fe−N6	115.48(6)	113.04(7)	N3−Fe1−N3	78.82(13)	82.69(11)	82.98(13)
N3−Fe1−N1	85.43(6)	86.60(7)	N3−Fe1−N4	82.76(11)	83.55(8)	84.00(9)
				96.88(10)	94.81(8)	94.85(9)
N4−Fe1−N3	77.15(6)	77.50(7)	N1−N3−N3−N1	18.11(12)	13.97(8)	16.38(9)
N6−Fe1−N4	85.20(6)	85.63(7)				
N1−N3−N4−N6	23.52(8)	21.47(8)				

flash-cooled or slowly cooled from room-temperature to 110 K, significant crystal damage occurred, and diffraction was of poor quality (most likely due to a destructive solid−solid phase transition occurring between 200 and 110 K). Thus, the structure of **11c** could only be determined at 200 K. The structure of the solvated compound $[Fe(\mathbf{3})(NCSe)_2]\cdot MeOH$ (**11c′**) could be determined at 110 K as no crystal damage occurred upon cooling. Dark red and almost black single crystals of compounds **13c** and **16c**, respectively, were also obtained. X-ray structure determination showed that the crystal lattices of both **13c** and **16c** are solvent free. The structures of the LS (low-spin) and HS (high-spin) phases of **13c** were determined both at 110 and 300 K since no significant loss of crystallinity occurred upon cooling. The structure of **16c** was only determined at 110 K, since the temperature necessary to obtain the HS state is too high for collecting data with the temperature controller that was used for single crystal X-ray crystallography (see below). The crystal structures of **11c**, **11c′**, **13c** (LS phase only), and **16c** are shown in Figure 1. In all cases, the tetradentate R_2bapbpy ligand was found to be coordinated to iron(II) in the basal plane, leaving the two selenocyanate ligands in *trans* positions of the octahedron (Figure 1). Selected bond lengths and angles are provided in Table 2.

For **11c**, the average Fe−N bond length is ca. 2.16 Å, which is typical of a HS Fe(II) complex in the FeN_6 octahedral environment. The large discrepancy in *cis* N−Fe1−N basal

dx.doi.org/10.1021/ic502381m | *Inorg. Chem.* 2014, 53, 13162−13173

coordination angles, as well as the torsion angle N1−N3−N4−N6 (23.52(8)°) (Table 2), suggest that the octahedral geometry is strongly distorted. For the solvated compound **11c**′, the average Fe−N bond length is found to be 2.13 Å, which is slightly shorter than that found in **11c** but still suggests an HS Fe(II) complex. The *cis* N−Fe1−N angles in the basal plane of the ligand bapbpy lie between 77.50(7)° and 113.04(7)° (Table 2), which is comparable to the molecular conformation found for the solvent-free compound **11c**. In the asymmetric unit of the solvated structure of **11c**′, the solvent molecule is H-bonded acceptor to one N−H bridge of the R_2bapbpy ligand via N−H···O hydrogen bond [N···O = 2.863(3) Å], and is H-bond donor to a neighboring $NCSe^-$ ligand via one intermolecular O−H···Se interaction [O···Se = 3.338(3) Å] (Supporting Information Figure S1).

In the structures of compounds **13c** and **16c**, the iron complexes are found at sites of 2-fold axial symmetry, and hence only halves of those complexes are crystallographically independent. For compound **13c**, the average Fe−N bond length was found to be 1.96 Å at 102(2) K, which is typical of a LS Fe(II) complex in an FeN_6 octahedral environment. At 300(2) K, the average Fe−N bond length for **13c** was found to be 2.13 Å, which is in agreement with a HS state. For compound **16c**, the average Fe−N bond length is 1.97 Å at 110(2) K, which suggests a LS Fe(II) complex in an FeN_6 octahedral environment. Furthermore, the *cis* N−Fe1−N basal coordination angles of **13c** and **16c** are very similar in their LS state (Table 2). In summary, the crystal structures of compounds **13c** and **16c** are relatively similar to each other, but also with the one observed for the compound [Fe(bapbpy)$(NCS)_2$].[25] In contrast the Fe complexes in the crystal structures of **11c** and **11c**′ feature a more distorted octahedron.

The crystal packing of compounds **11c**, **13c**, and **16c** is characterized by two sets of supramolecular interactions as shown in Figure 2. The first set includes weak N−H···Se intermolecular interactions occurring between two adjacent iron complexes along the crystallographic *c* axis. Unlike the N−H···S interactions found in the compound [Fe(bapbpy)$(NCS)_2$] for which each sulfur atom is involved in a single H-bond interaction,[25] only one of the two Se atoms (e.g., Se1 in Figure 2a) from the selenocyanate ligands in **11c** is a bifurcated acceptor in two N−H···Se hydrogen bonds. The two neighboring molecules found along *c* are donors via two N−H bridges. Crystals of the thiocyanate analogue of **11c**, [Fe(**3**)$(NCS)_2$], were also obtained by method **c**, and the crystal structure of [Fe(**3**)$(NCS)_2$] has been determined via single crystal X-ray crystallography (see Figures S2 and S3 and details in the Supporting Information). The structure of [Fe(**3**)$(NCS)_2$] has also very similar N−H···S hydrogen-bonding interactions to those found in the structure of **11c**, which suggests that the Me_2bapbpy ligand **3** is responsible for this specific packing. In **11c** the N···Se interatomic distance [3.5376(17) and 3.5398(17) Å] is close to the sum of the van der Waals radii (3.45 Å), which advocates for hydrogen-bonding interactions. In contrast, the N−H···Se intermolecular distances for compounds **13c** [4.0579(19) Å for the LS phase] and **16c** [3.968(2) Å] at 102 and 110 K, respectively, are significantly longer than 3.45 Å, which suggests much weaker N−H···Se intermolecular interactions for these compounds.

In all compounds a second set of intermolecular interactions is caused by $\pi-\pi$ stacking between the terminal pyridine rings of two adjacent molecules. The centroid−centroid distance is 4.074(12) Å for compound **11c** at 200 K (Table 3), while the

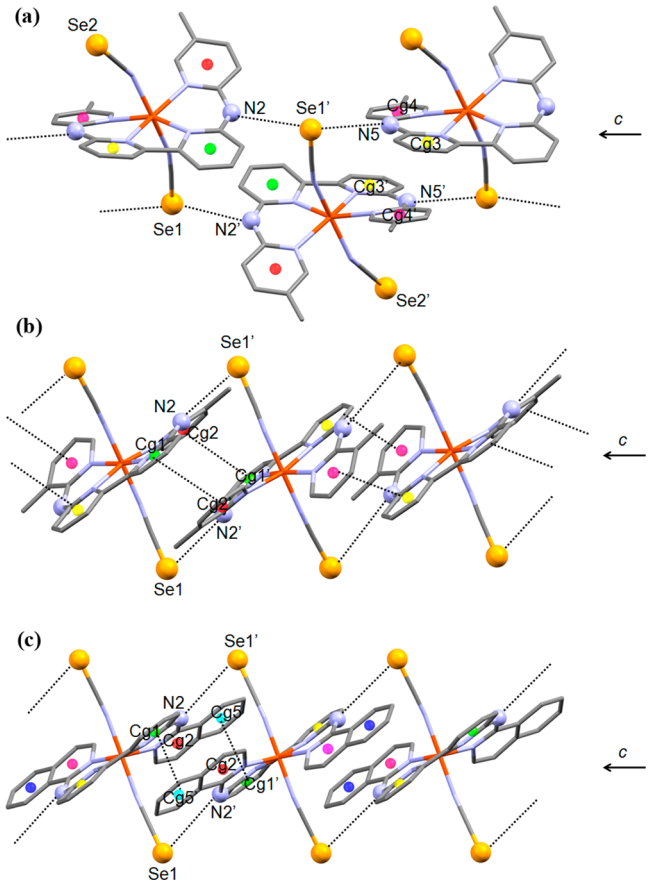

Figure 2. Crystal packing along the crystallographic *c* axis for compounds (a) **11c** at 200(2) K, (b) **13c** at 102(2) K, and (c) **16c** at 110(2) K. Symmetry operator: ′ = −*x*, −*y*, −*z*.

corresponding distance is 3.846(2) and 3.818(6) Å for **13c** at 300 and 102 K, respectively. For compound **16c**, each ring of the bipyridine fragment is involved in $\pi-\pi$ stacking with the two fused aromatic rings of the isoquinoline groups of the neighboring molecules, with centroid−centroid distances of 3.757(16) and 3.858(16) Å. Overall, $\pi-\pi$ stacking interactions are weak but similar within this family of compounds (**11c**, **13c**, and **16c**). In summary, compound **11c** shows stronger hydrogen-bonding interactions than **13c** and **16c**, and the selenocyanate compounds have almost identical molecular geometry and crystal packing compared to their thiocyanate analogues.

For the compounds obtained by methods **a**, **b**, or **c**, mass spectrometry indicated the presence of chemically identical complexes. However, SCO compounds are prone to polymorphism or lattice solvent inclusion (i.e., solvates).[22] For example, different crystallization conditions may lead to the crystallization of two chemically different materials [Fe(bapbpy)$(NCS)_2$] and [Fe(bapbpy)$(NCS)_2$]·2DMF.[27] Thus, molecular characterization methods are not sufficient, and the influence of the sample preparation methods on the structural phases and purity of compounds **9**, **11**, **13**, **15**, and **16** was investigated by powder X-ray diffraction (PXRD). The powder diffractograms for compounds **9a**, **9b** (Figure 3), **11a**, **11b**, **13a**, **13b**, **15a**, **15b** (Supporting Information Figure S4), and **16a** (Figure 3) were measured at room-temperature and compared to calculated diffractograms from the available crystal structures. For compounds **11**, **13**, and **15** the experimental (**11a** vs **11b**, **13a** vs **13b**, and **15a** vs **15b**) and calculated (**11c** or **13c**) powder

dx.doi.org/10.1021/ic502381m | *Inorg. Chem.* 2014, 53, 13162−13173

Table 3. N···Se Distances (Å), N−H···S Angles (deg), and Centroid−Centroid Distances (Å) Found in Complexes 11c, 13c, and 16c[a]

	11c	13c		16c
T (K)	200(2)	300(2)	102(2)	110(2)
phase	HS	HS	LS	LS
N2···Se1′	3.5376(17)	4.238(3)	4.0579(19)	3.968(2)
N5···Se1′	3.5398(17)	n.a.	n.a.	n.a.
N2−H2A···Se1′	171(2)	165(3)	161(2)	166(2)
N5−H5A···Se1′	174(2)	n.a.	n.a.	n.a.
Cg2···Cg1′	7.549(14)	3.846(2)	3.818(6)	3.858(16)
Cg3···Cg4′	4.074(12)	3.846(2)	3.818(6)	3.858(16)
Cg5···Cg1′	n.a.	n.a.	n.a.	3.757(16)

[a]n.a. = non applicable. Symmetry operator ′ = $-x$, $-y$, $-z$.

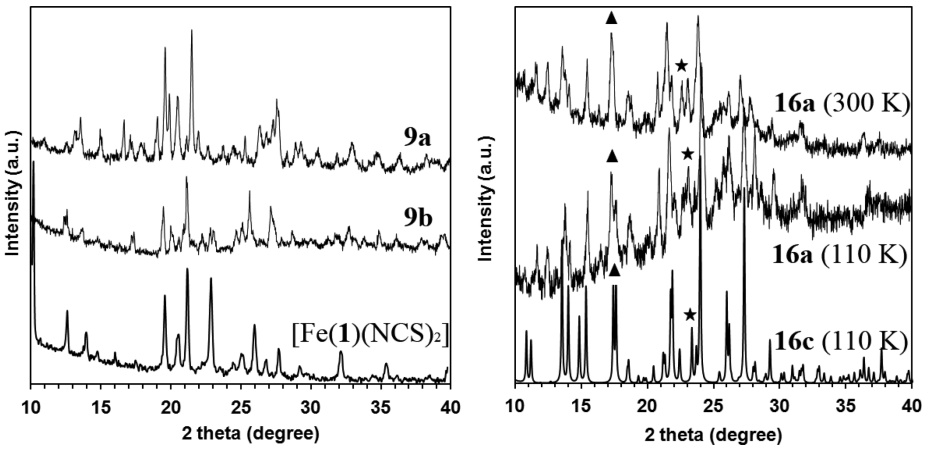

Figure 3. Left: Powder X-ray diffractograms at room-temperature for compounds **9a**, **9b**, and [Fe(**1**)$(NCS)_2$] prepared by method **a**.[25] Right: Powder X-ray diffractograms of compound **16a** at 300 and 110 K, and calculated diffractograms from the single X-ray structure of compound **16c** at 110 K.

diffractograms show no major differences, thus demonstrating that for ligands **3**, **5** and **7** all preparation methods lead to the same chemical compound with no sign of polymorphism. In particular, the powder diffractograms of **15a** and **15b** match well that of [Fe(**7**)$(NCS)_2$] (Supporting Information Figure S4), which demonstrates that both selenocyanate and thiocyanate materials for ligand 7 crystallize similarly. For compound **16a**, the powder diffractogram was measured at both 110 and 300 K (Figure 3). The diffractogram of **16a** at 300 K shows significant changes compared to 110 K, for example, a single peak at $2\theta \approx 17.3°$ (▲ in Figure 3) at 300 K turns to two close peaks at low-temperatures, and two peaks at $2\theta \approx 22.6°$ become a single peak at 110 K (★). These changes suggest that the compound undergoes a phase transition upon cooling. In addition, there were no major differences between the calculated spectrum from the crystal structure of **16c** (LS phase) and the measured diffractogram of **16a** at 110 K, which concluded that compounds **16a** and **16c** are the same materials.

In contrast, comparison of the experimental powder X-ray diffractograms of compounds **9a** and **9b** at room-temperature clearly shows different structures (Figure 3). The major differences are (i) the intense reflection at $2\theta \approx 21.5°$ for compound **9a**, which is shifted slightly in **9b**; (ii) some reflections of **9a**, *e.g.*, at $2\theta \approx 19.1°$, 16.7°, and 17.8°, that are absent in **9b**; (iii) multiple reflection peaks between $2\theta \approx 26.3°$ and 27.6° in **9a** appear to be a single peak for **9b**. Thus, **9a** and **9b** are clearly two different materials. This result is consistent with the elemental analysis for **9b**, which showed the best fit with two DMF solvent molecules per iron complex in the crystal lattice, whereas **9a** has not been in contact with DMF at all. Additionally, the powder diffractogram of **9a** is clearly different from that of its thiocyanate analogue [Fe(**1**)$(NCS)_2$][25] (also prepared via method **a**), which shows that, for the bapbpy complex, changing thiocyanates to selenocyanates leads to significant structural changes in the crystal lattice. Unfortunately, all efforts to grow single crystals of **9c** turned out to be unsuccessful. In summary, PXRD proves that the different methods of preparation produce the same material for compounds **11**, **13**, **15**, and **16**. However, the materials prepared via the two different methods **a** and **b** for compound **9** have different structures that also differ from that of [Fe(**1**)-$(NCS)_2$].

Magnetic Susceptibility Measurements. Magnetic susceptibility measurements were carried out to investigate the SCO properties of compounds **9**−**16**. According to $\chi_M T$ versus T plots (χ_M stands for the molar magnetic susceptibility and T the temperature, see Supporting Information, Figure S5), between 30 and 300 K the $\chi_M T$ values of **10a**, **12a**, and **14a** stay constant at a value slightly lower than 3.3 cm^3 K mol^{-1}, the value usually expected for HS iron(II) complexes in an octahedral coordination sphere, for which an orbital momentum contribution usually adds up to the spin-only value of 3.0 cm^3 K mol^{-1}. These low $\chi_M T$ values confirm the lower chemical purity of samples of type a, as already noticed by elemental analysis for compound **9** and **11** (see above). There is thus no spin crossover for **10a**, **12a**, and **14a**. On the other hand, both samples of type a and b for compounds **9**, **11**, **13**, **15**, and **16** show SCO properties (see Figure 4 and Table 4). The $\chi_M T$ versus T curves for **13b** and **15b** were essentially similar to those of **13a** and **15a**, which

dx.doi.org/10.1021/ic502381m | Inorg. Chem. 2014, 53, 13162−13173

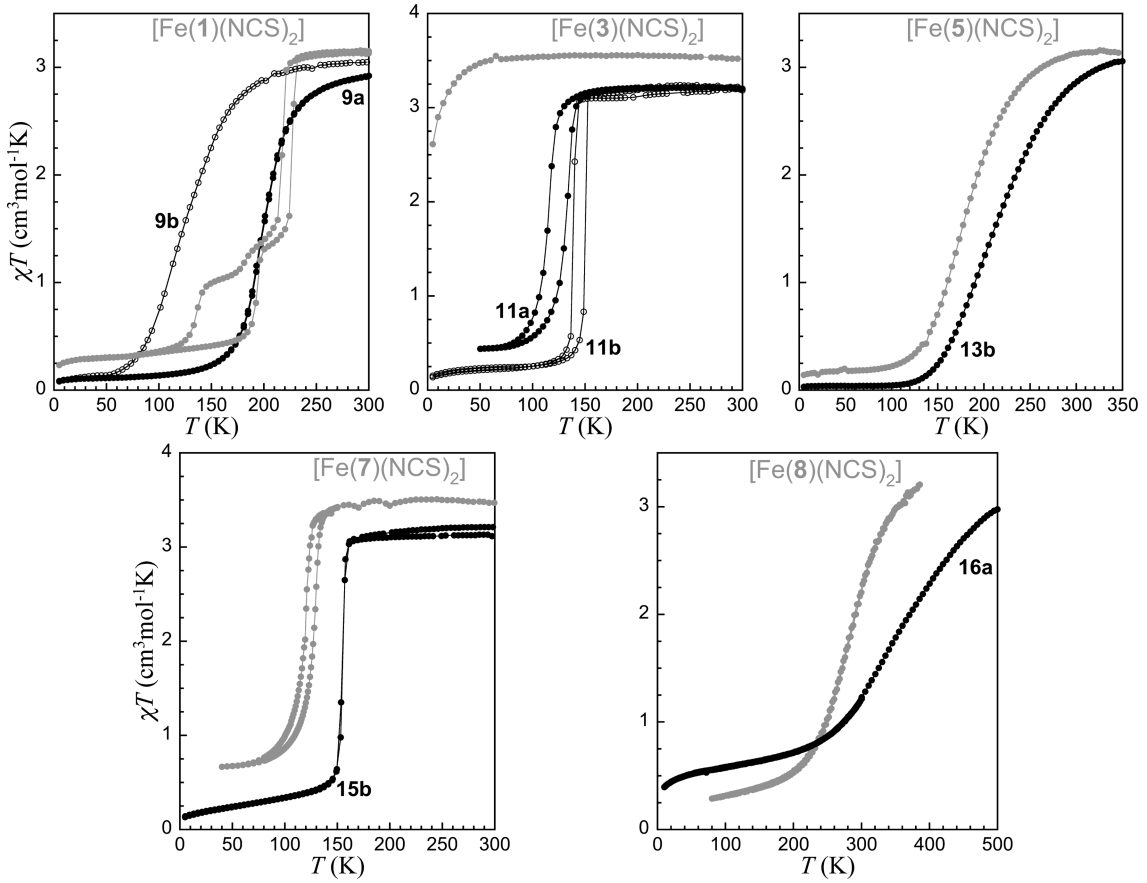

Figure 4. Comparison of the $\chi_M T$ vs T curves of compounds **9a** and **9b**, **11a** and **11b**, **13b**, **15b**, and **16a** to those of their thiocyanate analogues (full gray dots).[26] Heating/cooling rate is ~1 K min^{-1}.

Table 4. Transition Temperatures As Derived from the Maxima in d($\chi_M T$)/dT and Hysteresis Widths for the SCO Compounds [Fe(L)(NCSe)$_2$] with Heating/Cooling Rate = 0.3−1.1 K min^{-1}

compd	$T_{1/2}\downarrow$ (K) or $T_{1/2}$	$T_{1/2}\uparrow$ (K)	ΔT_{hyst}[a] (K)
9a	195(4)		
9b	113(4)		
11a	113(4)	137(4)	24(6)
11b	136(4)	153(4)	17(6)
13a	213(16)		
13b	201(4)		
15a	145(4)		
15b	154(4)		
16a	357(19)		

[a]Only indicated when $T_{1/2}\uparrow - T_{1/2}\downarrow$ is larger than the uncertainty on $T_{1/2}$.

confirmed that the materials obtained by method **a** or **b** were similar for ligands **5**, and **7**. Minor variations in the transition temperatures and lower $\chi_M T$ values (Table 4) at room- or low-temperatures were attributed to the higher chemical purity of samples prepared by method **b**. In contrast, a dramatic decrease of the transition temperature of $\Delta T_{1/2}$ = 82(4) K is observed from **9a**, whose transition temperature is 195(4) K as measured from the maximum of d($\chi_M T$)/dT, to **9b**, the transition being in both cases gradual and complete from ca. 3.0 cm^3 K mol^{-1} at 300 K to 0.1 cm^3 K mol^{-1} at 5 K. This observation is consistent with what has been found from elemental analyses and PXRD data, which all point to the different chemical nature of the SCO materials **9a** and **9b**. The difference between **9a** and **9b** is reminiscent of what has been observed with the thiocyanate analogue, where two crystallographically characterized compounds [Fe(**1**)(NCS)$_2$] and [Fe(**1**)(NCS)$_2$]·2DMF are obtained from two different preparation methods.[27]

For compound **11a** the $\chi_M T$ value of 3.2 cm^3 K mol^{-1} at 300 K diminishes down to a plateau at *ca.* 0.5 cm^3 K mol^{-1} below 70 K, in an almost complete and abrupt SCO. The transition temperatures of 113(4) K in the cooling mode and 137(4) K in the heating mode (Table 4) open a hysteresis cycle of 24(6) K indicative of high cooperativity. Compound **11b** has similar behavior albeit with a more complete transition and the hysteresis reduced to 17(6) K and shifted to higher temperatures (Figure 4 and Table 4). For compound **13b** $\chi_M T$ gradually decreased from 3.0 cm^3 K mol^{-1} at 350 K down to 0.1 cm^3 K mol^{-1} at 5 K, thus showing a noncooperative SCO, centered at 202(4) K. Compound **15b** exhibits an abrupt and complete SCO at 154(4) K with no significant hysteresis. Finally for compound **16a** a $\chi_M T$ value of 1.2 cm^3 K mol^{-1} was measured at 300 K indicating a mixture of HS and LS state. An oven was used to probe the magnetic susceptibility of compound **16a** between 300 and 500 K. At 500 K the $\chi_M T$ value of 2.9 is close to the expected value of 3.0 cm^3 K mol^{-1} so that the SCO can be estimated as being almost complete. The $\chi_M T$ value gradually decreases from 500 to 100 K, with a transition temperature estimated to be 357(19) K. This value is significantly higher than that found for the thiocyanate analogue [Fe(**8**)(NCS)$_2$] (288 K).[26] Compound

dx.doi.org/10.1021/ic502381m | *Inorg. Chem.* 2014, 53, 13162−13173

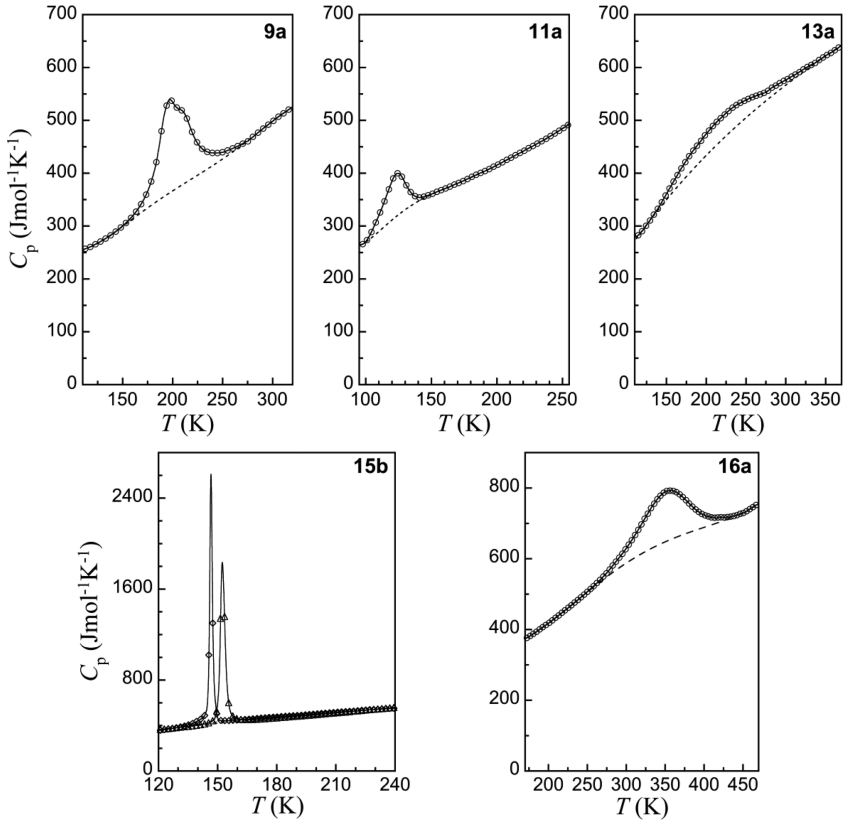

Figure 5. Molar heat capacities of compounds **9a**, **11a**, **13a**, **15b**, and **16a**, as derived from differential scanning calorimetry. Data in both warming and cooling are shown for **15b**. Dashed lines are estimates of normal heat capacities used for ΔC_p determination. Heating/cooling rate is 10 K min^{-1}.

16a has the highest reported transition temperature of all iron(II) bapbpy-based SCO materials.

DSC Measurements. Calorimetric measurements on SCO compounds provide important thermodynamic parameters such as the enthalpy and entropy variations accompanying a spin transition, and the transition temperature, and they provide quantitative indications on the cooperativity of the transition. Thus, the molar heat capacities at constant pressure C_p were measured for compounds **9**, **11**, **13**, **15b**, and **16**, by differential scanning calorimetry (DSC, see Figure 5). Compounds **15a** and **15b** are the same material, but **15b** is higher in purity; therefore, DSC data are shown for **15b** only. The transition of **9b** reaches temperatures that are too low for our setup and thus could not be measured. The excess heat capacity, ΔC_p, due to the spin crossover in the above-mentioned compounds was obtained by estimating normal heat-capacity curve with the high- and low-temperature data, which are shown as dashed lines in Figure 5, and subtracting it from the total heat capacity (Figure 6). In this estimation, no heat-capacity step at the transition temperature was considered. Compound **9a** showed a broad heat capacity anomaly between 150 and 300 K, culminating at 200 K. This temperature matches well with that determined by the magnetic susceptibility measurements ($T_{1/2}$ = 195(4) K). For compound **11a**, the DSC measurements were performed in the heating mode only due to the closeness of the transition temperature $T_{1/2}\downarrow$ to the low-temperature limit of the DSC setup. Compound **11a** showed a broad heat capacity anomaly between 100 and 150 K, with a maximum estimated at 125 K, which is slightly lower than that given by magnetic susceptibility measurements ($T_{1/2}\uparrow$ = 137(4) K). For compound **13a**, a very broad heat capacity anomaly is observed between 150 and 300 K, with its maximum estimated at 220 K. This is again consistent with the magnetic susceptibility measurements of **13a**, which show a gradual SCO

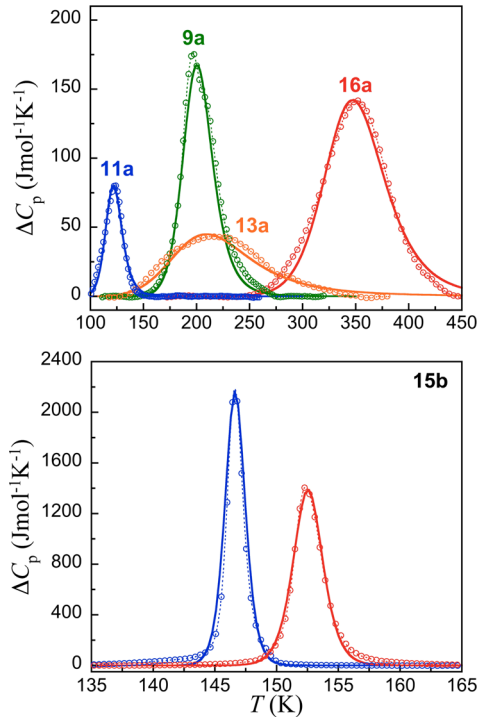

Figure 6. Excess molar heat capacities of compounds **9a**, **11a**, **13a**, and **16a** upon warming (top) and **15b** in both warming and cooling modes (bottom, respectively in red/blue). Full lines are fits to the domain model (see text and Table 5).

dx.doi.org/10.1021/ic502381m | *Inorg. Chem.* 2014, 53, 13162−13173

curve with $T_{1/2}$ estimated at about 214(20) K. For compound **15b**, DSC measurements in both cooling and heating modes exhibited sharp heat-capacity peaks centered at ca. 146 and 153 K, respectively, in agreement with the magnetic measurements of **15b**, although no hysteresis is observed in the $\chi_M T$ versus T curve, which may be associated with the DSC measurements performed at a much higher temperature scan rate of 10 K min^{-1}. Finally, for compound **16a**, a broad heat capacity anomaly was observed between 300 and 450 K, the maximum being at 350 K. Overall, DSC data are in good agreement with the magnetic susceptibility measurements for all tested compounds.

As done previously for the thiocyanate series,[26] the phenomenological domain model proposed by Sorai[28,29] was used to quantify and compare the cooperative character of the SCO compounds presented in this work, through the number of interacting SCO molecules per domain, n. Thus, the experimental excess heat capacity data were fitted to eq 1 (full lines in Figure 6), fixing the excess enthalpy due to the SCO, $\Delta_{SCO}H$, to the value derived experimentally (see Table 5). The resulting best-fit parameters n and $T_{1/2}$ are gathered in Table 5. Clearly the values for n correlate with the differences in abruptness of the SCO curves in magnetic susceptibility measurements or sharpness of heat capacity peaks. Both compounds **11a** and **15b** can be considered as cooperative SCO compounds with values of n of 14.4 and 54.8/70.5 (in cooling/warming mode), respectively, whereas compounds **9a**, **13a**, and **16a** have lower n values (5.8, 3.1, and 4.8, respectively) and can be considered as weakly cooperative.

Table 5. Excess Enthalpy and Entropy Due to the SCO, and Parameters Describing the SCO ($T_{1/2}$) and Its Cooperativity (n) in Compounds 9a, 11a, 13a, 15b, and 16a As Derived from Sorai's Domain Model (See Text)

compd	9a	11a	13a	15b	16a
$\Delta_{SCO}H$ (kJ mol^{-1})	6.24	1.66	4.73	4.43/4.69	10.9
$\Delta_{SCO}S$ (J mol^{-1} K^{-1})	31.0	13.7	22.0	30.2/30.7	31.5
n	5.8	14.4	3.1	54.8/70.5	4.8
$T_{1/2}$ (K)	202	123	222	153/147	351

$$\Delta C_p = \frac{n(\Delta_{SCO}H)^2}{RT^2} \frac{\exp\left[\frac{n\Delta_{SCO}H}{R}\left(\frac{1}{T} - \frac{1}{T_{1/2}}\right)\right]}{\left\{1 + \exp\left[\frac{n\Delta_{SCO}H}{R}\left(\frac{1}{T} - \frac{1}{T_{1/2}}\right)\right]\right\}^2} \quad (1)$$

DISCUSSION

Many research groups have compared iron(II) bis(thiocyanate)-based SCO molecular compounds and their selenocyanate analogues.[19,20,23,30−45] Although the difference in electronegativity between selenium (2.55 on the Pauling scale) and sulfur (2.58) is not large, it is usually used to justify the stabilization of the LS state and increase in SCO transition temperature observed with selenocyanates ligands, compared with thiocyanate ligands. Our series of [Fe(R_2bapbpy)(NCX)$_2$] compounds follow the expected trend (see Figure 4), and in the case of [Fe(**3**)(NCX)$_2$] replacement of the thiocyanate ligands by selenocyanates turns a HS compound into the SCO compound **11a**.

The influence of S to Se replacement on cooperativity has been less systematically addressed. Usually, bis(selenocyanato) compounds were shown to be less cooperative than their bis(thiocyanato) analogues. For example, Sorai measured n = 95 for [Fe(phen)$_2$(NCS)$_2$] and n = 77 for [Fe(phen)$_2$(NCSe)$_2$].[28] In more recent studies, Klingele et al. reported two examples of two-step bis(thiocyanato) molecular SCO compounds that become one-step upon replacement of sulfur by selenium.[23,24] In most studies, the sulfur and selenium atoms are not involved in hydrogen-bonding interactions, as the other ligands in the coordination sphere are deprived of H-bond donor groups. In such cases the lower cooperativity with selenocyanate ions is usually attributed to the more diffuse charge of the Se atom (larger atomic radii for a similar charge density), which weakens intermolecular interactions and results in less efficient propagation of local structural changes accompanying SCO. However, the interplay between hydrogen bonds and cooperativity is discussed very actively in the spin-crossover field.[46−49] In the series of compounds **9**−**16**, the presence of N−H donor bridges within the tetrapyridyl ligand structure in principle allows for establishing hydrogen bonds with the acceptor chalcogenide atoms. Thus, S-to-Se substitution was expected to significantly influence the cooperativity of the SCO.

According to our results in the series [Fe(R_2bapbpy)(NCX)$_2$] the substitution of S by Se does not usually generate significant structural changes in the crystal lattice; i.e., for ligands **3**, **5**, **7**, and **8** (Supporting Information Figure S4c and S6), the thiocyanate and selenocyanate compounds are isostructural. Compound **9a** seems to be the outlier of the series, as the PXRD data of the sulfur and selenium analogues are clearly different (Figure 3). In the absence of more information on the crystal structure of **9a**, its noncooperative SCO cannot be compared to the highly cooperative SCO of [Fe(bapbpy)(NCS)$_2$].[25] Except for this compound, the qualitative model of cooperativity developed with the thiocyanate analogues [Fe(R_2bapbpy)(NCS)$_2$] still holds for the selenocyanato analogues.[26] In the absence of substituents in β,β'-positions on the terminal pyridine rings of the tetrapyridyl ligand (Scheme 1), the SCO of the iron bis(selenocyanate) compound remains cooperative (compounds **11** and **15**) due to the N−H···Se hydrogen-bonding interactions characterized crystallographically in **11c**. In contrast, the N−H···Se intermolecular distances for **13c** and **16c** are significantly longer than those found in **11c**, which in our model is due to the hindering substituents located near the NH bridges of the R_2bapbpy ligand. Such weakened N−H···Se interactions correlate with the noncooperative SCO observed for these compounds. Thus, N−H···Se hydrogen-bonding networks indeed play a prominent role in the cooperativity of the SCO of [Fe(R_2bapbpy)(NCX)$_2$] compounds.

However, the only SCO compounds of the [Fe(R_2bapbpy)-(NCX)$_2$] series for which the crystal structures for both X = S and X = Se are known and can be compared, are noncooperative. For these compounds the n values of the selenocyanate analogues are similarly low (n = 3.1 for **13a** and 4.8 for **16a**) compared to those of their thiocyanate analogues (n = 2.8 and 5.3, respectively). With ligand **3**, which has no β,β' substituent, only the selenocyanate compound has SCO properties, so that its (high) n value cannot be compared with that of the thiocyanate analogue. Overall, the only ligand deprived of β,β' substituent and for which both iron complexes have SCO properties is ligand **7**. Unfortunately this ligand is highly insoluble, which prevents crystallization of any of the [Fe(**7**)(NCX)$_2$] compounds. Powder diffraction studies do indicate that both analogues have almost identical structures (Supporting Information Figure S4). For these two compounds a significant increase of n was observed

dx.doi.org/10.1021/ic502381m | Inorg. Chem. 2014, 53, 13162−13173

with selenocyanate ligands (**15a**, n = 54.8) compared to thiocyanates (n = 16.8). This case appears as a rather unique example for which the S-to-Se replacement *increases* cooperativity. In principle, indeed, N−H···X hydrogen bonding, and thus cooperativity, should be weaker with X = Se than with X = S, as the negative charge on the selenium atom is lower than that on sulfur.[50,51] We hypothesize that structural effects might play a role in this compound: if the intermolecular N···Se and N···S distances are almost identical, the larger ionic radius of Se (184 pm) compared to S (170 pm) might increase the strength of the N−H···Se hydrogen-bonding network, leading to higher cooperativity compared to the thiocyanate case. Alternatively, other intermolecular interactions may play a role (e.g., $\pi-\pi$ stacking), which will only be discovered by obtaining the crystal structures of both compounds.

CONCLUSION

Within the eight selenocyanate compounds of the [Fe(R_2bapbpy)$(NCSe)_2$] series **9**−**16**, five have SCO properties and two are cooperative with hysteresis cycles (**11** and **15**) whereas the others (**9**, **13**, **16**) are noncooperative. With the exception of **9**, which cannot be compared to [Fe(**1**)$(NCS)_2$] as it has a different crystal structure, striking structural similarities were observed between the thiocyanate and selenocyanate analogues. In all known crystal structures of this type of complex the chalcogenide atoms play an important role in the hydrogen-bonding network, as in all compounds short N···X intermolecular distances correlate with cooperative SCO behavior. For noncooperative SCO compounds (**13**, **16**) the expected increase of the transition temperature upon S-to-Se substitution was observed without noticeable change of the cooperativity. For the cooperative compounds **15**, an increase of the n value, i.e., an increase of the cooperativity, is observed compared to the thiocyanate analogue. Overall this study suggests that using selenocyanate ligands not only allows for increasing the transition temperature of SCO, but also for increasing cooperativity, provided N−H···Se hydrogen bond intermolecular interactions are present in the crystal structure.

EXPERIMENTAL SECTION

General. All reactions were performed under argon atmosphere using standard Schlenk line techniques. Toluene was dried over sodium and degassed, diethyl ether was dried over sodium and benzophenone, and DMF was dried over CaH_2. Degassed solvents were obtained by bubbling argon through 50 mL of solvent in a Schlenk flask for 1 h. For all complex syntheses, degassed solvents were used. The reagent 6,6′-dibromo-2,2′-bipyridine was synthesized in two steps according to the literature,[52] and the syntheses of the bapbpy derivatives **1**−**8** followed previously described procedures.[26] All other reagents obtained from commercial sources were used without further purification. Filtration of the iron(II) compounds was done on Whatman membrane filters (regenerated cellulose RC55) with 1 μm pores. ^{1}H NMR and ^{13}C NMR spectra were recorded at room-temperature using a Bruker DPX300 (300 MHz) spectrometer. Chemical shifts are indicated in ppm relative to TMS. Infrared spectra (IR) were taken on a PerkinElmer FT-IR spectrometer Paragon 1000 equipped with a Golden Gate ATR device, using the reflectance technique (4000−300 cm^{-1}, resolution 4 cm^{-1}). Mass spectrometry was performed on a Finnigan Mat 900 spectrometer equipped with an electrospray interface. HR mass spectra were measured using direct injection (2 μL of a 2 μM solution in DMF and 0.1% formic acid) on a Thermo Finnigan LTQ Orbitrap mass spectrometer equipped with an electronspray ion source in positive mode (source voltage 3.5 kV, sheath gas flow 10, capillary temperature 275 °C) with resolution = 60.000 at m/z = 400 (mass range =150−2000) and dioctylphtalate (m/z = 391.28428) as "lock mass". Elemental analyses (C, H, N, S) were obtained from a PerkinElmer 2400 Series II analyzer.

Powder X-ray diffraction data were collected on a Philips X'Pert PRO diffractometer equipped with the X'celerator using Cu Kα radiation. Single crystal X-ray diffraction data were collected by measuring all reflection intensities using either a KM4/Xcalibur (detector: Sapphire3) with enhanced graphite-monochromated Mo Kα radiation (λ = 0.710 73 Å) for compounds **13c** (LS and HS phases), **16c**, and [Fe(**3**)$(NCS)_2$] or a SuperNova diffractometer (equipped with Atlas detector) with Cu Kα radiation (λ = 1.541 78 Å) for compounds **11c** and **11c**′ under the program CrysAlisPro [versions 1.171.35.11 (2011) or 1.171.36.24 (2012), Agilent Technologies]. The program CrysAlisPro was used to refine the cell dimensions and for data reduction. The structures were solved with the program SHELXS-97 or SHELXS-2013[53] and were refined on F^2 with SHELXL-97 or SHELXL-2013.[53] Analytical numeric absorption corrections based on a multifaceted crystal model were applied using CrysAlisPro. The temperature of the data collection was controlled using the system Cryojet (manufactured by Oxford Instruments). The H atoms (except when specified) were placed at calculated positions using the instructions AFIX 43 or 137 with isotropic displacement parameters having values 1.2 or 1.5 times U_{eq} of the attached C atoms. The H atoms attached to N2, N5 (**11c**, **11c**′, and [Fe(**3**)$(NCS)_2$]), and O1S (**11c**′) were found from difference Fourier maps, and their coordinates/isotropic factors were refined freely [the N−H and O−H distances were restrained using the DFIX instructions]. All structures are ordered.

Magnetic susceptibility measurements were performed using a Quantum Design MPMS-5S SQUID magnetometer for compounds **9a**, **10a**, **11a**, **12a**, **13a**, **14a**, **15a**, **9b**, **11b**, **13b**, and **15b**. In each case, the ∼10−20 mg sample was mounted on a plastic straw before introduction in the magnetometer. Direct current magnetization measurements were performed in a field of 0.1 T, from 300 to 5 K (cooling mode) and from 5 to 300 K (heating mode) with a rate 0.3−1.1 K min^{-1}. The total measuring time for each sample was 20 h. Compound **16a** was measured using a Quantum Design MPMS-XL magnetometer at the Physical Measurements unit of the Servico de Apoyo a la Investigación-SAI, Universidad de Zaragoza. The measurements in the range 300−500 K were performed with the oven option. For these the powder sample (15.25 mg) was mounted in a piece of Al foil (22.66 mg) that was folded in a round shape, and held/trapped into the knot formed by 4 constantan fibers. Corrections for the sample holder assemblies were applied, as well as corrections for the diamagnetism of the sample, calculated using Pascal's constants.[54] All compounds were treated as pure compounds, including the less pure samples of type a, which sometimes results, for the least soluble ligands, in $\chi_M T$ values at high temperatures that are slightly lower than 3.0 cm^3 K mol^{-1}. Heat capacities were obtained by use of a differential scanning calorimeter Q1000 with the LNCS accessory from TA Instruments. The temperature and enthalpy scales were calibrated with a standard sample of indium, using its melting transition (156.6 °C, 3296 J mol^{-1}). The measurements were carried out using 6−13 mg of samples sealed in aluminum pans with mechanical crimp, with an empty pan as reference. The zero-heat flow procedure described by TA Instruments was followed, using as reference compound a synthetic sapphire. Using this procedure, an overall accuracy of ca. 0.2 K in temperature and up to 5−10% in the heat capacity is estimated over the whole temperature range.

Synthesis of Iron(II) Complexes. The 0.1 M methanolic solution of [Fe$(NCSe)_2$] used for the synthesis of the iron complexes was prepared as follows: $FeSO_4{\cdot}xH_2O$ (99.999% trace metals basis, CAS nr. 13463-43-9) (151 mg, 1.0 mmol), and KSeCN (288 mg, 2.0 mmol) were mixed in degassed methanol (6 mL) and stirred for 40 min. Ascorbic acid (5 mg) was added to prevent aerial oxidation. K_2SO_4 was removed by filtration on filter paper (Whatman 597) into a 10 mL volumetric flask. The flask was filled up to 10 mL with methanol, resulting in a clear, colorless iron(II) solution, which must be used within 1 h. Oxidation of the iron solution upon aging was visible due to a change of color (from colorless to dark violet).

Three methods were used to synthesize the iron(II) complexes [Fe(L)$(NCSe)_2$]: (the compound numbers with notation **a**, **b**, or **c**, are indicated for the corresponding synthetic methods)

dx.doi.org/10.1021/ic502381m | Inorg. Chem. 2014, 53, 13162−13173

*Method **a**.* In a two-necked round-bottom flask the tetrapyridyl ligand (0.1 mmol) and 3 mL of degassed methanol were added to form a suspension. The 0.1 M methanolic solution of $[Fe(NCSe)_2]$ (1.1 equiv) was then added resulting in an immediate color change. The suspension was stirred at room-temperature under argon for 16 h. The solids were filtered through a membrane filter, thoroughly washed with methanol, and dried under vacuum for 3 h.

*Method **b**.* In a two-necked round-bottom flask the tetrapyridyl ligand (0.05 mmol) was dissolved in an appropriate amount of degassed DMF (in the case of **15b**, ligand **7** was heated in DMF to 130 °C to be dissolved and then cooled down to room-temperature). A 0.1 M methanolic solution of $[Fe(NCSe)_2]$ (1.1 equiv) was added at room-temperature. The resultant solution was left unstirred overnight under argon. In the case of ligands **1**, **3**, and **5**, solids appeared at the bottom of the flask within a day. For ligand **7** this was not the case, and excess MeOH was carefully layered on top of the DMF solution, to obtain a precipitate the next day. In all cases, the excess solution was removed by cannula, and the solid was thoroughly washed with methanol and dried under high vacuum for 3 h to obtain compounds **9b**, **11b**, **13b**, or **15b**.

During the synthesis of compounds **10b**, **12b**, and **14b**, no solid appeared overnight after addition of $Fe(NCSe)_2$. However, with addition of excess MeOH (20 mL), solids appeared within 3 days. In each case, the IR spectrum was identical to that of free ligand **2**, **4**, and **6**, respectively. Compound **16b** could not be prepared since ligand **8** has very low solubility in DMF, even when heated.

*Method **c**.* The ligand **3** or **5** (20 mg) was dissolved in dry and degassed DMF (4 mL), affording a clear yellow/orange solution to which a small amount (~5 mg) of ascorbic acid was added to prevent oxidation. In the case of ligand **8** (24 mg), the DMF suspension (5 mL) was heated to 80 °C and cooled down to room-temperature; however, the ligand was still not fully dissolved. The 1 mL aliquots of ligand solution were pipet-filtered over 1 cm of Celite into a Corning tube. $[Fe(NCSe)_2]$ (0.1 M methanolic solution, 136 μL for ligand **3** or **5**, 114 μL for ligand **8**, 1.1 equiv) was carefully layered on top of the ligand solution. Degassed methanol was then layered on top of these two layers. The four tubes were then sealed and left untouched. Red/dark crystals were obtained for compounds **11c**, **11c′**, **13c**, and **16c** within a week by liquid−liquid diffusion.

Important Note on Crystal Growing. Visible light seems to play a role in the crystallization of this family of compounds. For example, sunny weeks were systematically followed by significantly increased yield and crystal quality, whereas controlled crystal growing experiments performed in the dark or during weeks of bad weather always led to much lower crystal quality crystals or no crystals at all. Crystal growth should be best achieved during sunny periods.

*[Fe(**1**)(NCSe)$_2$] (**9a**).* The red powder was obtained with a yield of 83%. IR spectroscopy (cm^{-1}): 3188, 3101, 2090 ($NCSe^-$), 2057 ($NCSe^-$), 1622, 1582, 1558, 1527, 1482, 1460, 1441, 1436, 1345, 1237, 1175, 1165, 1134, 1074, 1060, 1010, 1004, 915, 862, 794, 765, 734, 668, 645, 630, 614, 599, 512, 482, 418, 342, 324. High resolution ES-MS from DMF solution m/z (calcd): 501.9978 (501.9978 $[M - NCSe]^+$). Anal. Calcd (%) for $C_{22}H_{16}FeN_8Se_2 \cdot 0.6C_{20}H_{16}N_6$: C 50.39, H 3.18, N 20.05. Found: C 51.06, H 2.21, N 19.95.

*[Fe(**1**)(NCSe)$_2$]·2DMF (**9b**).* The small red polycrystals were obtained with a yield of 67%. IR spectroscopy (cm^{-1}): 3313, 3205, 3077, 3014, 2928, 2067 ($NCSe^-$), 1661 (DMF), 1652, 1646, 1582, 1558, 1538, 1482, 1462, 1436, 1428, 1387, 1368, 1281, 1242, 1173, 1159, 1134, 1102, 1057, 1006, 868, 843, 797, 768, 681, 666, 645, 614, 578, 516, 488, 422, 414, 355, 324. High resolution ES-MS from DMF solution m/z (calcd): 501.9973 (501.9978 $[M - NCSe]^+$). Anal Calcd (%) for $C_{28}H_{30}FeN_{10}O_2Se_2$: C 44.68, H 4.02, N 18.62. Found: C 44.30, H 4.03, N 18.65.

*[Fe(**2**)(NCSe)$_2$] (**10a**).* The brown powder was obtained with a yield of 93%. IR spectroscopy (cm^{-1}): 3052, 2806, 2057 ($NCSe^-$), 1664, 1630, 1610, 1576, 1560, 1534, 1514, 1465, 1442, 1383, 1341, 1296, 1270, 1245, 1176, 1158, 1091, 1039, 1000, 988, 960, 890, 861, 805, 774, 746, 725, 720, 670, 640, 570, 495, 428. High resolution ES-MS from DMF solution m/z (calcd): 530.0288 (530.0291 $[M - NCSe]^+$).

*[Fe(**3**)(NCSe)$_2$] (**11a**).* The orange powder was obtained with a yield of 82%. IR spectroscopy (cm^{-1}): 3278, 3197, 3108, 2094 ($NCSe^-$), 2060 ($NCSe^-$), 1626, 1616, 1581, 1558, 1527, 1496, 1456, 1436, 1410, 1374, 1236, 1177, 1149, 1048, 1002, 894, 821, 791, 736, 668, 654, 638, 512, 483, 425, 323. ESI-MS (DMF) m/z (calcd): 530.1 (530.0 $[M - NCSe]^+$). Anal. Calcd (%) for $C_{24}H_{20}FeN_8Se_2$: C 45.45, H 3.18, N 17.67. Found: C 43.50, H 2.08, N 16.20.

*[Fe(**3**)(NCSe)$_2$] (**11b**).* The small red polycrystals were obtained with a yield of 28%. IR spectroscopy (cm^{-1}): 3277, 3193, 3103, 2093 ($NCSe^-$), 2052 ($NCSe^-$), 1652, 1625, 1581, 1558, 1526, 1496, 1456, 1436, 1410, 1373, 1226, 1176, 1148, 1047, 1001, 894, 820, 790, 736, 652, 638, 512, 484, 452, 418, 319. High resolution ES-MS from DMF solution m/z (calcd): 530.0290 (530.0291 $[M - NCSe]^+$). Anal. Calcd (%) for $C_{24}H_{20}FeN_8Se_2$: C 45.43, H 3.18, N 17.67. Found: C 45.06, H 2.65, N 17.34.

*[Fe(**3**)(NCSe)$_2$] and [Fe(**3**)(NCSe)$_2$]·MeOH (**11c** and **11c′**).* Two types of single crystals were obtained upon using method **c**, with a total yield of 51%.

Crystal data for **11c**: fw = 634.25, red plate, 0.34 × 0.25 × 0.11 mm^3, triclinic, $P\bar{1}$ (No. 2), a = 8.6403(3) Å, b = 11.2005(4) Å, c = 13.5845(5) Å, α = 68.946(3)°, β = 79.002(3)°, γ = 80.171(3)°, V = 1196.84(8) $Å^3$, Z = 2, D_x = 1.760 g cm^{-3}, μ = 8.782 mm^{-1}, abs corr range 0.193−0.501. The 14 037 reflections were measured up to a resolution of $(\sin\theta/\lambda)_{max}$ = 0.62 $Å^{-1}$. There were 4684 unique reflections (R_{int} = 0.0187), of which 4561 were observed $[I > 2\sigma(I)]$. The 327 parameters were refined using 2 restraints. R1/wR2 $[I > 2\sigma(I)]$: 0.0248/0.0652. R1/wR2 [all reflns]: 0.0255/0.0656. S = 1.015. Residual electron density found between −0.60 and 0.46 e $Å^{-3}$.

Crystal data for **11c′**: fw = 666.29, dark red plate, 0.34 × 0.16 × 0.06 mm^3, triclinic, $P\bar{1}$ (No. 2), a = 9.0074(3) Å, b = 11.3214(3) Å, c = 13.6382(3) Å, α = 75.312(2)°, β = 89.534(2)°, γ = 81.410(2)°, V = 1329.59(7) $Å^3$, Z = 2, D_x = 1.664 g cm^{-3}, μ = 7.965 mm^{-1}, abs corr range 0.163−0.639. The 17 736 reflections were measured up to a resolution of $(\sin\theta/\lambda)_{max}$ = 0.62 $Å^{-1}$. There were 5202 unique reflections (R_{int} = 0.0246), of which 5015 were observed $[I > 2\sigma(I)]$. The 350 parameters were refined using 3 restraints. R1/wR2 $[I > 2\sigma(I)]$: 0.0282/0.0744. R1/wR2 [all reflns]: 0.0293/0.0755. S = 1.041. Residual electron density found between −0.68 and 0.69 e $Å^{-3}$.

*[Fe(**4**)(NCSe)$_2$] (**12a**).* The reddish orange powder was obtained with a yield of 90%. IR spectroscopy (cm^{-1}): 3289, 3192, 3100, 2080 ($NCSe^-$), 1634, 1593, 1580, 1558, 1532, 1490, 1463, 1442, 1436, 1418, 1371, 1290, 1236, 1224, 1193, 1174, 1137, 1031, 1010, 934, 866, 815, 802, 788, 734, 690, 668, 644, 624, 588, 543, 487, 453, 425, 330. ESI-MS (DMF) m/z (calcd): 530.1 (530.03 $[M - NCSe]^+$).

*[Fe(**5**)(NCSe)$_2$] (**13a**).* The brown powder was obtained with a yield of 68%. IR spectroscopy (cm^{-1}): 3386, 3072, 2100 ($NCSe^-$), 2070 ($NCSe^-$), 1616, 1586, 1576, 1558, 1532, 1520, 1506, 1471, 1447, 1436, 1418, 1362, 1312, 1227, 1191, 1176, 1118, 1076, 1006, 920, 813, 788, 750, 668, 648, 624, 584, 542, 425, 327. High resolution ES-MS from DMF solution m/z (calcd): 530.0282 (530.0291 $[M - NCSe]^+$). Anal. Calcd (%) for $C_{24}H_{20}FeN_8Se_2$: C 45.43, H 3.18, N 17.67. Found: C 45.56, H 2.51, N 17.58.

*[Fe(**5**)(NCSe)$_2$] (**13b**).* The dark brown powder was obtained with a yield of 44%. IR spectroscopy (cm^{-1}): 3382, 3074, 2100 ($NCSe^-$), 2066 ($NCSe^-$), 1668, 1652, 1646, 1616, 1586, 1558, 1531, 1520, 1506, 1464, 1447, 1436, 1418, 1361, 1312, 1225, 1190, 1175, 1117, 1074, 1030, 1006, 920, 896, 812, 787, 749, 734, 668, 648, 623, 582, 541, 487, 450, 426, 327. High resolution ES-MS from DMF solution m/z (calcd): 530.0294 (530.0291 $[M - NCSe]^+$). Anal. Calcd (%) for $C_{24}H_{20}FeN_8Se_2$: C 45.43, H 3.18, N 17.67. Found: C 45.05, H 2.47, N 17.52.

*[Fe(**5**)(NCSe)$_2$] (**13c**).* Dark single crystals were obtained with a yield of 40%. Crystal data for **13c**: Phase I (102(2) K): fw = 634.25, dark red irregular shape crystal, 0.31 × 0.09 × 0.06 mm^3, monoclinic, $C2/c$ (No. 15), a = 13.2071(3) Å, b = 13.3999(3) Å, c = 14.0838(3) Å, β = 105.467(2)°, V = 2402.20(9) $Å^3$, Z = 4, D_x = 1.754 g cm^{-3}, μ = 3.689 mm^{-1}, abs corr range: 0.534−0.858. The 10 051 reflections were measured up to a resolution of $(\sin\theta/\lambda)_{max}$ = 0.62 $Å^{-1}$. There were 2429 unique reflections (R_{int} = 0.0288), of which 2181 were observed $[I > 2\sigma(I)]$. The 164 parameters were refined using 1 restraint. R1/wR2 $[I > 2\sigma(I)]$: 0.0240/0.0596. R1/wR2 [all reflns]: 0.0289/0.0615. S = 1.076. Residual electron density was found between −0.33 and 0.53 e $Å^{-3}$. Phase II (300(2) K): fw = 634.25, dark red irregular shape crystal, 0.31 ×

dx.doi.org/10.1021/ic502381m | *Inorg. Chem.* 2014, 53, 13162−13173

0.09 × 0.06 mm^3, monoclinic, $C2/c$ (No. 15), a = 13.4237(3) Å, b = 13.3663(4) Å, c = 14.2028(5) Å, β = 101.916(3)°, V = 2493.43(13) Å^3, Z = 4, D_x = 1.690 g cm^{-3}, μ = 3.554 mm^{-1}, abs corr range: 0.549−0.839. The 7254 reflections were measured up to a resolution of $(\sin\theta/\lambda)_{max}$ = 0.59 Å^{-1}. There were 2193 unique reflections (R_{int} = 0.0279), of which 1820 were observed [$I > 2\sigma(I)$]. The 164 parameters were refined using 1 restraint. R1/wR2 [$I > 2\sigma(I)$]: 0.0351/0.0841. R1/wR2 [all reflns]: 0.0459/0.0894. S = 1.039. Residual electron density was found between −0.35 and 0.49 e Å^{-3}.

*[Fe(**6**)(NCSe)$_2$] (**14a**).* The rusty yellow powder was obtained with a yield of 88%. IR spectroscopy (cm^{-1}): 3301, 3214, 3066, 2078 (NCSe$^-$) 1652, 1616, 1600, 1582, 1558, 1538, 1506, 1483, 1464, 1456, 1436, 1404, 1299, 1255, 1174, 1146, 1004, 824, 798, 780, 753, 668, 644, 618, 524, 486, 418, 398, 328. ESI-MS (DMF) m/z (calcd): 602.1 (602.03 [M − NCSe]$^+$).

*[Fe(**7**)(NCSe)$_2$] (**15a**).* The reddish orange powder was obtained with a yield of 83%. IR spectroscopy (cm^{-1}): 3258, 3058, 2061 (NCSe$^-$), 1634, 1612, 1576, 1558, 1538, 1490, 1456, 1445, 1418, 1404, 1362, 1322, 1280, 1259, 1248, 1219, 1188, 1172, 1149, 1004, 986, 962, 866, 784, 758, 735, 685, 668, 638, 544, 462, 423, 397, 357, 328. High resolution ES-MS from DMF solution m/z (calcd): 602.0287 (602.0292 [M − NCSe]$^+$), 730.9380 (730.9390 [M + Na]$^+$).

*[Fe(**7**)(NCSe)$_2$] (**15b**).* The brown powder was obtained with yield of 35%. IR spectroscopy (cm^{-1}): 3290, 3058, 2060 (NCSe$^-$), 1634, 1615, 1576, 1539, 1490, 1445, 1404, 1361, 1322, 1279, 1245, 1218, 1189, 1171, 1148, 1003, 986, 913, 866, 785, 743, 685, 662, 635, 540, 461, 427, 356, 309. High resolution ES-MS from DMF solution m/z (calcd): 602.0286 (602.0292 [M − NCSe]$^+$). Anal. Calcd (%) for $C_{30}H_{20}FeN_8Se_2$: C 51.02, H 2.85, N 15.86. Found: C 52.98, H 2.83, N 15.96.

*[Fe(**8**)(NCSe)$_2$] (**16a**).* The brown powder was obtained with yield of 81%. IR spectroscopy (cm^{-1}): 3364, 3058, 2108 (NCSe$^-$), 2072 (NCSe$^-$), 1635, 1611, 1592, 1576, 1558, 1532, 1506, 1496, 1471, 1464, 1456, 1436, 1418, 1394, 1347, 1303, 1256, 1232, 1169, 1148, 1077, 1026, 986, 860, 794, 739, 684, 668, 662, 618, 581, 524, 492, 468, 412, 398, 340, 314. High resolution ES-MS from DMF solution m/z (calcd): 602.0290 (602.0292 [M − NCSe]$^+$).

*[Fe(**8**)(NCSe)$_2$] (**16c**).* Dark crystals were obtained and sent immediately for single crystal X-ray structure determination. IR spectroscopy (cm^{-1}): 3368, 3066, 2108 (NCSe$^-$), 2074 (NCSe$^-$), 1635, 1610, 1591, 1576, 1558, 1538, 1532, 1506, 1464, 1436, 1418, 1394, 1312, 1286, 1232, 1168, 1029, 983, 858, 807, 793, 739, 668, 662, 581, 538, 492, 469, 418, 375, 350, 336, 322, 313.

Crystal data for **16c** follow: fw = 706.31, black block, 0.28 × 0.17 × 0.15 mm^3, monoclinic, $C2/c$ (No. 15), a = 13.0310(2) Å, b = 14.0929(3) Å, c = 14.6490(3) Å, β = 94.4729(15)°, V = 2682.02(9) Å^3, Z = 4, D_x = 1.749 g cm^{-3}, μ = 3.315 mm^{-1}, abs corr range: 0.510−0.673. The 8173 reflections were measured up to a resolution of $(\sin\theta/\lambda)_{max}$ = 0.62 Å^{-1}. There were 2703 unique reflections (R_{int} = 0.0465), of which 2338 were observed [$I > 2\sigma(I)$]. The 190 parameters were refined using 1 restraint. R1/wR2 [$I > 2\sigma(I)$]: 0.0340/0.0929. R1/wR2 [all reflns]: 0.0407/0.0964. S = 1.044. Residual electron density found between −0.81 and 1.07 e Å^{-3}.

■ ASSOCIATED CONTENT

Supporting Information

Crystallographic data in CIF format. Hydrogen-bonding interactions in the crystal packing of compound **11c**′, description of the crystal structure and packing of [Fe(**3**)(NCS)$_2$], $\chi_M T$ vs T curves for compounds **10a**, **12a**, and **14a** in both heating and cooling modes, powder X-ray diffractograms for compounds **11**, **13**, and **15**, and a MOLDEN-generated superposition of the crystal structures of compounds **11**, **13**, and **16** with their corresponding thiocyanate analogues. This material is available free of charge via the Internet at http://pubs.acs.org.

■ AUTHOR INFORMATION

Corresponding Author

*E-mail: bonnet@chem.leidenuniv.nl.

Notes

The authors declare no competing financial interest.

■ ACKNOWLEDGMENTS

Prof. Dr. Elisabeth Bouwman is acknowledged for critical reading of the manuscript and scientific discussions.

■ REFERENCES

(1) Southon, P. D.; Liu, L.; Fellows, E. A.; Price, D. J.; Halder, G. J.; Chapman, K. W.; Moubaraki, B.; Murray, K. S.; Létard, J. F.; Kepert, C. J. *J. Am. Chem. Soc.* **2009**, *131*, 10998−11009.
(2) Ohba, M.; Yoneda, K.; Agusti, G.; Muñoz, M. C.; Gaspar, A. B.; Real, J. A.; Yamasaki, M.; Ando, H.; Nakao, Y.; Sakaki, S.; Kitagawa, S. *Angew. Chem., Int. Ed.* **2009**, *48*, 4767−4771.
(3) Coronado, E.; Giménez-Marqués, M.; Espallargas, G. M.; Brammer, L. *Nat. Commun.* **2012**, *3*, 828.
(4) Mcdaniel, A. M.; Klug, C. M.; Shores, M. P. *Eur. J. Inorg. Chem.* **2013**, *2013*, 943−950.
(5) Ni, Z.; Mcdaniel, A. M.; Shores, M. P. *Chem. Sci.* **2010**, *1*, 615−621.
(6) Salmon, L.; Molnár, G.; Zitouni, D.; Quintero, C.; Bergaud, C.; Micheau, J. C.; Bousseksou, A. *J. Mater. Chem.* **2010**, *20*, 5499−5503.
(7) Shepherd, H. J.; Gural'skiy, I. y. A.; Quintero, C. M.; Tricard, S.; Salmon, L.; Molnár, G.; Bousseksou, A. *Nat. Commun.* **2013**, *4*, 2607.
(8) Alam, M. S.; Stocker, M.; Gieb, K.; Müller, P.; Haryono, M.; Student, K.; Grohmann, A. *Angew. Chem., Int. Ed.* **2010**, *49*, 1159−1163.
(9) Cavallini, M.; Bergenti, I.; Milita, S.; Ruani, G.; Salitros, I.; Qu, Z. R.; Chandrasekar, R.; Ruben, M. *Angew. Chem., Int. Ed.* **2008**, *47*, 8596−8600.
(10) Kahn, O.; Krober, J.; Jay, C. *Adv. Mater.* **1992**, *4*, 718−728.
(11) Liu, T.; Zheng, H.; Kang, S.; Shiota, Y.; Hayami, S.; Mito, M.; Sato, O.; Yoshizawa, K.; Kanegawa, S.; Duan, C. *Nat. Commun.* **2013**, *4*, 2826.
(12) Létard, J. F.; Guionneau, P.; Goux-Capes, L. *Top. Curr. Chem.* **2004**, *235*, 221−249.
(13) Kahn, O.; Martinez, C. J. *Science* **1998**, *279*, 44−48.
(14) Bousseksou, A.; Molnár, G.; Salmon, L.; Nicolazzi, W. *Chem. Soc. Rev.* **2011**, *40*, 3313−3335.
(15) Gütlich, P.; Hauser, A.; Spiering, H. *Angew. Chem., Int. Ed.* **1994**, *33*, 2024−2054.
(16) Halcrow, M. A. *Chem. Soc. Rev.* **2011**, *40*, 4119−4142.
(17) Gütlich, P.; Goodwin, H. A. *Top. Curr. Chem.* **2004**, *233*, 1−47.
(18) Baker, W. A.; Bobonich, H. M. *Inorg. Chem.* **1964**, *3*, 1184−1188.
(19) Konig, E.; Madeja, K.; Watson, K. J. *J. Am. Chem. Soc.* **1968**, *90*, 1146−1153.
(20) Konig, E.; Madeja, K. *Chem. Commun.* **1966**, 61−62.
(21) Ozarowski, A.; Yu, S. Z.; McGarvey, B. R.; Mislankar, A.; Drake, J. E. *Inorg. Chem.* **1991**, *30*, 3167−3174.
(22) Real, J. A.; Gaspar, A. B.; Muñoz, M. C. *Dalton Trans.* **2005**, 2062−2079.
(23) Klingele, J.; Kaase, D.; Schmucker, M.; Lan, Y.; Chastanet, G.; Létard, J.-F. *Inorg. Chem.* **2013**, *52*, 6000−6010.
(24) Klingele, J.; Kaase, D.; Klingele, M. H.; Lach, J. *Dalton Trans.* **2012**, *41*, 1397−1406.
(25) Bonnet, S.; Siegler, M. A.; Costa, J. S.; Molnár, G.; Bousseksou, A.; Spek, A. L.; Gamez, P.; Reedijk, J. *Chem. Commun.* **2008**, 5619−5621.
(26) Arcís-Castillo, Z.; Zheng, S.; Siegler, M. A.; Roubeau, O.; Bedoui, S.; Bonnet, S. *Chem.—Eur. J.* **2011**, *17*, 14826−14836.
(27) Bonnet, S.; Molnár, G.; Costa, J. S.; Siegler, M. A.; Spek, A. L.; Bousseksou, A.; Fu, W. T.; Gamez, P.; Reedijk, J. *Chem. Mater.* **2009**, *21*, 1123−1136.
(28) Sorai, M.; Seki, S. *J. Phys. Chem. Solids* **1974**, *35*, 555−570.
(29) Sorai, M.; Nakazawa, Y.; Nakano, M.; Miyazaki, Y. *Chem. Rev.* **2013**, *113*, PR41−122.
(30) Adams, C. J.; Haddow, M. F.; Harding, D. J.; Podesta, T. J.; Waddington, R. E. *CrystEngComm* **2011**, *13*, 4909−4914.
(31) Adams, C. J.; Muñoz, M. C.; Waddington, R. E.; Real, J. A. *Inorg. Chem.* **2011**, *50*, 10633−10642.

(32) Chen, X.-Y.; Huang, R.-B.; Zheng, L.-S.; Tao, J. *Inorg. Chem.* **2014**, *53*, 5246−5252.
(33) Chilton, N. F.; Gass, I. A.; Moubaraki, B.; Chastanet, G. *Dalton Trans.* **2013**, *42*, 16494−16509.
(34) Gaspar, A. B.; Muñoz, M. C.; Moliner, N.; Ksenofontov, V.; Levchenko, G.; Gütlich, P.; Real, J. A. *Monatsh. Chem.* **2003**, *134*, 169−178.
(35) Gobeze, W. A.; Milway, V. A.; Olguín, J.; Jameson, G. N. L.; Brooker, S. *Inorg. Chem.* **2012**, *51*, 9056−9065.
(36) Hayami, S.; Kawajiri, R.; Juhasz, G.; Kawahara, T.; Hashiguchi, K.; Sato, O.; Inoue, K.; Maeda, Y. *Bull. Chem. Soc. Jpn.* **2003**, *76*, 1207−1213.
(37) Moliner, N.; Muñoz, M. C.; Létard, S.; Létard, J. F.; Solans, X.; Burriel, R.; Castro, M.; Kahn, O.; Real, J. A. *Inorg. Chim. Acta* **1999**, *291*, 279−288.
(38) Neville, S. M.; Leita, B. A.; Halder, G. J.; Kepert, C. J.; Moubaraki, B.; Létard, J.-F.; Murray, K. S. *Chem.—Eur. J.* **2008**, *14*, 10123−10133.
(39) Arcís-Castillo, Z.; Piñeiro-López, L.; Muñoz, M. C.; Ballesteros, R.; Abarca, B.; Real, J. A. *CrystEngComm* **2013**, *15*, 3455−3462.
(40) Tao, J.-Q.; Gu, Z.-G.; Wang, T.-W.; Yang, Q.-F.; Zuo, J.-L.; You, X.-Z. *Inorg. Chim. Acta* **2007**, *360*, 4125−4132.
(41) Wannarit, N.; Roubeau, O.; Youngme, S.; Teat, S. J.; Gamez, P. *Dalton Trans.* **2013**, *42*, 7120−7130.
(42) Bréfuel, N.; Shova, S.; Lipkowski, J.; Tuchagues, J.-P. *Chem. Mater.* **2006**, *18*, 5467−5479.
(43) Real, J. A.; Castro, I.; Bousseksou, A.; Verdaguer, M.; Burriel, R.; Castro, M.; Linarès, J.; Varret, F. *Inorg. Chem.* **1997**, *36*, 455−464.
(44) Real, J. A.; Bolvin, H.; Bousseksou, A.; Dworkin, A.; Kahn, O.; Varret, F.; Zarembowitch, J. *J. Am. Chem. Soc.* **1992**, *114*, 4650−4658.
(45) Moliner, N.; Muñoz, M. C.; van Koningsbruggen, P. J.; Real, J. A. *Inorg. Chim. Acta* **1998**, *274*, 1−6.
(46) Lochenie, C.; Bauer, W.; Railliet, A. P.; Schlamp, S.; Garcia, Y.; Weber, B. *Inorg. Chem.* **2014**, DOI: 10.1021/ic501624b.
(47) Schlamp, S.; Weber, B.; Naik, A. D.; Garcia, Y. *Chem. Commun.* **2011**, *47*, 7152−7154.
(48) Weber, B.; Bauer, W.; Pfaffeneder, T.; Dîrtu, M. M.; Naik, A. D.; Rotaru, A.; Garcia, Y. *Eur. J. Inorg. Chem.* **2011**, *2011*, 3193−3206.
(49) Salmon, L.; Donnadieu, B.; Bousseksou, A.; Tuchagues, J.-P. *C. R. Acad. Sci. Paris IIc* **2010**, *2*, 305−309.
(50) Schultz, P. W. *Mol. Phys.* **1996**, *88*, 217−246.
(51) Schultz, P. W.; Leroi, G. E.; Popov, A. I. *J. Am. Chem. Soc.* **1996**, *118*, 10617−10625.
(52) Bai, X. L.; Liu, X. D.; Wang, M.; Kang, C. Q.; Gao, L. X. *Synthesis* **2005**, 458−464.
(53) Sheldrick, G. M.; Schneider, T. R. *Methods Enzymol.* **1997**, *277*, 319−343.
(54) Bain, G. A.; Berry, J. F. *J. Chem. Educ.* **2008**, *85*, 532−536.